Geophysical Research Letters

RESEARCH LETTER
10.1029/2025GL116651

Evaluating the Influence of Traffic Congestion on Surface Urban Heat Island Intensity

Jangho Lee[1] and Max Berkelhammer[1]

[1]Earth and Environmental Sciences, University of Illinois Chicago, Chicago, IL, USA

Key Points:

- The surface urban heat island (SUHII) effect in Chicago shows a strong diurnal and weekly cycle
- The magnitude of SUHII increases by ~0.36°C per 10 mph reduction in bus speeds—a proxy for traffic congestion
- In dense-vegetated, low-building areas of the city, the coupling of traffic congestion and SUHII is more pronounced

Correspondence to:
J. Lee,
jholee@uic.edu

Citation:
Lee, J., & Berkelhammer, M. (2025). Evaluating the influence of traffic congestion on surface urban heat island intensity. *Geophysical Research Letters*, *52*, e2025GL116651. https://doi.org/10.1029/2025GL116651

Received 21 APR 2025
Accepted 29 JUL 2025

Abstract This study quantifies how traffic congestion influences the surface urban heat island intensity (SUHII) in Chicago using GOES LST data and Chicago Transit Authority (CTA) bus speed data. While SUHII is characterized by a well pronounced diurnal cycle that peaks around noon, we observed changes in strength of SUHII that were correlated with changes in traffic speed. This leads to distinct weekend and rush hour effects on SUHII. Citywide, we observed a statistically significant correlation in which each 10 mph decrease in bus speed is associated with an increase of 0.36°C in SUHII. That effect is stronger in highly vegetated, low-building areas, where traffic-emitted waste heat is more dominant than other anthropogenic sources. These findings highlight the importance of incorporating congestion metrics into urban heat research, offering new insights for planners and policymakers seeking to mitigate local thermal extremes.

Plain Language Summary We measured how traffic congestion affects Chicago's surface urban heat island (SUHII) using satellite data and bus speeds. SUHII peaks around midday. Traffic slows during the weekend and rush-hour. Looking at the relationship between the SUHII and the bus speeds, we find that each 10 mph drop in speed increases SUHII by 0.36°C—especially in areas with more trees and fewer buildings, where vehicle heat dominates. Our findings highlight the need to consider congestion in urban heat research, offering planners new ways to reduce local heat extremes and traffic demands.

1. Introduction

Urbanization has significantly altered natural environments worldwide, with the Urban Heat Island (UHI) effect being one of the most extensively studied consequences (Deilami et al., 2018; S. W. Kim & Brown, 2021; Rizwan et al., 2008). UHI describes the temperature disparity between urban centers and their surrounding rural or non-urban areas, primarily caused by the replacement of vegetated, permeable surfaces with artificial materials that retain heat. As metropolitan regions have expanded in both population and spatial extent over recent decades, the UHI phenomenon has intensified, leading to increased energy consumption (Baniassadi & Sailor, 2018; Lee & Dessler, 2022; Li et al., 2019; Morakinyo et al., 2019), heightened health risks during extreme heat events (F. Chen et al., 2023; Ebi et al., 2021; Lee & Dessler, 2023; Khosla et al., 2021), and added strain on urban infrastructure (Baniassadi et al., 2018; Singh et al., 2021; Zhang et al., 2019).

A particular branch of UHI research focuses on the Surface Urban Heat Island (SUHI), which is derived from land surface temperature (LST) measurements. SUHI arises from several well-understood processes linked to urban form and design. Common city materials such as concrete and asphalt generally have lower albedos and higher heat capacities than natural surfaces, absorbing large amounts of solar radiation during the day and releasing heat slowly at night. This effect is exacerbated by the dense, compact layout of cities, where narrow streets and closely packed buildings create urban canyons that trap heat and limit airflow, reducing opportunities for cooling (Hou et al., 2023; W. Peng et al., 2022; Shao et al., 2023). Additionally, the reduction in vegetative cover weakens evapotranspiration, further diminishing natural cooling mechanisms (Cui et al., 2021; Paschalis et al., 2021). Road networks, with their expansive surfaces and low reflectivity, frequently emerge as thermal hotspots, particularly during high-traffic periods when tailpipe emissions, engine heat, and frictional heating contribute to localized warming (Patriota et al., 2024; Sen, 2025).

While the role of impervious surfaces and building density in exacerbating SUHI has been studied at length, traffic congestion has received limited attention as a direct and quantifiable contributor to SUHI dynamics. Husni et al. (2022) analyzed the contribution of vehicle counts to CUHI, but their approach relied heavily on modeling the internal combustion heat from engines. Louiza et al. (2015) used a theoretical modeling framework to estimate transportation's impact on urban heat, while Teufel et al. (2021) employed a regional climate model incorporating

different anthropogenic heat sources—including traffic—to evaluate their localized weather effects. Yang et al. (2022) found that traffic restrictions during the Olympic Games reduced Beijing's UHI, although this was an isolated event rather than a persistent scenario for modeling the effects of traffic.

As congestion is a defining feature of many urban transportation networks—particularly in large cities with dense road systems and frequent commuting—understanding its role in amplifying SUHI is becoming increasingly important. However, most existing studies rely on modeling or isolated events, and there remains a notable gap in real data-driven research that examines traffic's contribution to SUHI during typical, day-to-day conditions in major cities. Additionally, the interplay of traffic congestion with other anthropogenic heat sources—such as waste heat from buildings and industry—and the extent to which high-resolution temporal variations in traffic patterns affect localized SUHI remain poorly understood. Addressing these gaps will require more comprehensive data sets, finer-scale analyses, and integration of multiple data streams to capture the full complexity of urban heat dynamics.

This study focuses on the city of Chicago, Illinois, which is the third-largest city in the U.S. with ∼2.7 million residents. The city routinely experiences hot, humid summers, and intense heat waves have historically posed significant public health challenges (Hayhoe et al., 2010; Klinenberg, 2015; Wilson & Chakraborty, 2019). A notable example is the 1995 Chicago heat wave (Kaiser et al., 2007), which resulted in hundreds of fatalities and prompted extensive research into urban heat vulnerability. In recent decades, increasing evidence suggests that climate change could intensify future heat events, making Chicago's heat mitigation strategies all the more important. Furthermore, Chicago is a major metropolis characterized by a robust transportation framework. Chicago's road network encompasses a variety of traffic conditions—from heavily trafficked downtown streets to suburban arterial roads, to expansive expressways that serve as vital commuter arteries.

This work pursues three primary objectives:

- Mapping SUHI and Traffic Patterns in Chicago: Using remote sensing data, we identify land surface temperature variations along with SUHI patterns and cycles. Simultaneously, we analyze traffic data to characterize the spatiotemporal dynamics of congestion across Chicago, establishing a foundation for comparing thermal anomalies with traffic behavior.
- Quantifying Traffic Congestion's Impact on SUHI: We assess the extent to which traffic congestion contributes to local SUHI intensity by integrating spatial and statistical methods to examine the relationship between surface temperatures and congestion metrics.
- Identifying Factors that Influence Traffic's SUHI Intensity: We investigate the conditions that mediate traffic-driven warming, such as tree cover, road width, and building area. Understanding these factors will help refine insights into where, when, and how traffic amplifies SUHI effects.

By addressing these objectives, this study aims to bridge the gap in knowledge concerning traffic-related heat emissions in everyday urban settings. Unlike studies focusing on isolated events or theoretical modeling, our real data-driven approach provides an empirical understanding of how routine traffic congestion contributes to SUHI. Moreover, examining various urban features—from vegetated cover to building morphology—allows us to distinguish how different aspects of the built environment can either mitigate or magnify traffic-induced warming. Ultimately, these insights not only enhance our understanding of SUHI dynamics but also guide more targeted interventions in urban planning, ranging from strategic tree planting to congestion management policies.

2. Data

2.1. Land Surface Temperature (LST) Data

The land surface temperature (LST) data used in this study is derived from the GOES-16, 17, and 18 satellites (collectively referred to as GOES) (Beale et al., 2019; Y. Yu & Yu, 2020; Y. Yu et al., 2008). Equipped with the Advanced Baseline Imager (ABI), these satellites record infrared measurements that are processed into LST products, maintaining an estimated error margin below 2°C (Y. Yu et al., 2011). GOES offers near-continuous coverage over North America at a 2 km spatial resolution and an hourly temporal resolution, allowing for detailed monitoring of diurnal temperature variations.

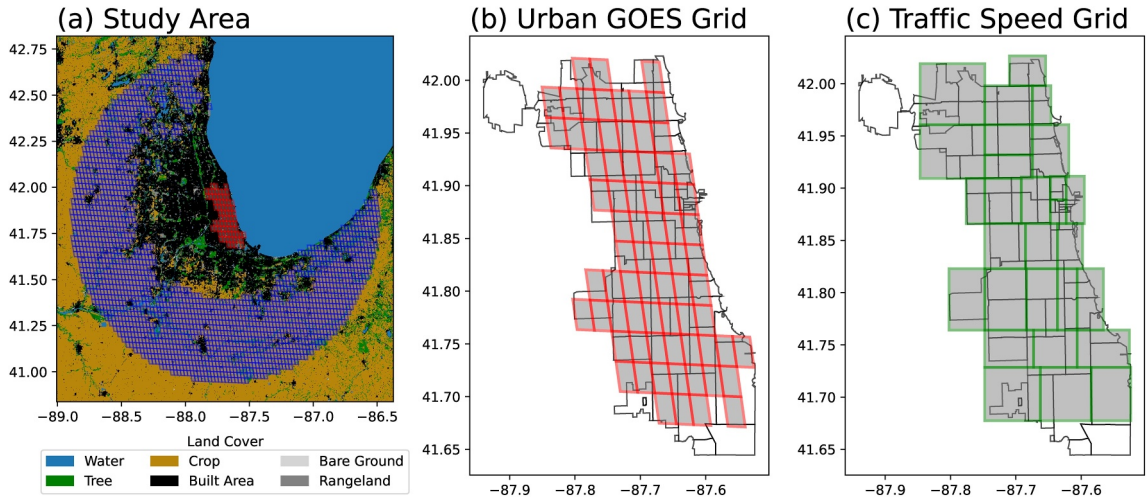

Figure 1. (a) Land cover map around the study region. The red grid boxes denote the urban grids used in this study, while the blue grid boxes represent the rural grids. (b) Detailed location of urban GOES grids (red) and zip code map of Chicago (black). (c) Boundaries of the urban traffic measurement area.

Although the spatial resolution of the GOES satellite (~2 km) is sufficient for analyzing the traffic data aggregated at a larger spatial scale, it is important to assess the sensitivity of these results against a higher-resolution LST product. To address this, we compared the GOES LST data with ECOSTRESS LST (~70 m) observations. Due to ECOSTRESS's non-geostationary orbit, only 145 clear scenes covering the Chicago region were available during the study period (less compared to coverage of GOES LST with over 20,000 scenes). Within these scenes, the mean absolute error (MAE) between GOES and ECOSTRESS LST was consistently below 0.5°C. Furthermore, the MAE for the calculated SUHI between these two data sets was less than 0.4°C, and notably, when aggregating the LST data to match traffic zone scales, the MAE remained below 0.4°C. In all comparisons, spatial correlations exceeded 0.9, confirming that the GOES LST product provides sufficient accuracy for our analysis. Nonetheless, we acknowledge that this sufficiency arises partly because our traffic data is averaged over relatively large spatial units; thus, more detailed studies using finer-scale traffic data might necessitate higher-resolution thermal observations.

This analysis presented here focuses on the warm season (May–September) from 2018 to 2024, a 7-year window in which SUHI effects are most prominent. By confining the data set to these months, we capture peak urban heat conditions and thereby ensure sufficient temporal and spatial variability to assess the influence of traffic congestion on SUHI patterns. Given that LST measurements are unavailable during cloudy conditions, we only include days where more than 75% of grid cells remain cloud-free, producing a data set that closely approximates clear-sky LST values. We only include hours where at least 75% of the GOES grid cells remain cloud-free. Hours failing this criterion are excluded from the analysis.

2.2. Land Cover Data and Urban to Rural Distinction

To delineate urban and rural areas for SUHI calculations, we use the 10 m resolution Sentinel-2 land cover data set, which annually classifies surface types including water, trees, flooded vegetation, crops, built areas, bare ground, snow/ice, clouds, and rangeland. Validation efforts for the Sentinel-2 land cover product indicate around 80% accuracy globally (Phiri et al., 2020; Rumora et al., 2020; Topaloğlu et al., 2016). Because Sentinel-2 land cover data are categorical, we identify the dominant land-cover type for each GOES cell by counting the occurrence of each category within that cell's 10 m pixels. The category with the highest count is assigned as the cell's representative land cover.

Urban areas are defined at GOES resolution within Chicago's main region, where traffic data is available. Rural reference areas are identified as non-urban, non-water grids within a 50–100 km radius of Chicago's urban center to exclude suburban influences while maintaining proximity for meaningful temperature comparisons. The selection of this range is typical for a megacity analysis (Kong et al., 2025; W. Liu et al., 2009; Luo et al., 2025). Figures 1a and 1b illustrate the resulting urban/rural classification and corresponding urban GOES grid.

2.3. Traffic Data

Figure 1c shows the boundaries of the urban traffic measurement zones derived from the Chicago Traffic Tracker data set, publicly available via the Chicago Data Portal. These traffic zones are defined at a spatial resolution of approximately 1–2 km, closely matching the spatial resolution (~2 km) of the GOES satellite data. Panel (c) explicitly illustrates the spatial alignment of the traffic speed data with the urban-rural land-cover classification (Figure 1a) and the urban GOES grid cells used for SUHII calculation (Figure 1b). This alignment ensures robust spatial integration among the traffic congestion, land-cover classification, and land surface temperature data sets.

The traffic data set itself provides average speed estimates of Chicago Transit Authority (CTA) buses aggregated every 10 min across the defined traffic zones. Given the extensive coverage of CTA bus routes across Chicago, bus speeds offer a reasonable proxy for overall traffic congestion: lower bus speeds generally indicate more congested streets. However, we acknowledge two limitations of this approach. First, streets without bus routes are not directly captured, which may exclude certain congestion hotspots—though this gap is partly mitigated by Chicago's dense bus network and grid street layout, where nearby roads typically share similar congestion levels. Second, the data set only covers the primary operational hours of CTA buses, approximately 6 a.m.–7 p.m., which limits observations to periods when bus frequency adequately reflects overall traffic conditions. While weekend data are included, they reflect fewer buses and shorter operating periods, which may not capture all weekend-specific congestion patterns. Future analyses integrating CTA bus data with private-vehicle speeds or GPS-based traffic data sets could more comprehensively capture congestion throughout the city.

To align the traffic data temporally and spatially with the GOES satellite observations, we aggregate bus speed data into hourly intervals and then spatially align them with the GOES grid cells. Specifically, we calculate a weighted average bus speed for each GOES cell by considering the proportion of each traffic zone falling within each cell. Both the traffic and GOES LST data sets are restricted to the same analysis period (6 a.m.–7 p.m.) to maintain consistent comparisons when examining the statistical relationship between traffic congestion and SUHII.

2.4. Auxiliary Data

We incorporate auxiliary data to refine our understanding of the urban landscape. First, we use NOAA's high-resolution regional land cover data set from the Coastal Change Analysis Program (C-CAP), which identifies canopy, impervious surfaces, and water bodies at a 1 m resolution using lidar and satellite imagery (NOAA, 2023). To match with the GOES grid, we aggregate these data by calculating the fraction of canopy pixels relative to the total number of pixels in each cell, effectively representing the proportion of land covered by trees.

However, canopy fraction alone captures only the areal extent of tree cover, so we also include a 250 m MODIS-based Enhanced Vegetation index (EVI) product (P.-Y. Chen et al., 2006; Justice et al., 2002; Son et al., 2014), computing an average EVI value over the study period for each GOES cell. This step captures additional vegetation characteristics (e.g., density) that may influence the local thermal environment.

Building footprint information is obtained from the Chicago Data Portal, where each polygon indicates a building's outline and number of floors. This allows us to determine the percentage of each GOES grid cell occupied by buildings. We also used the road network data set from Chicago Data Portal, which includes the geometry of roads and their respective lane counts. By summing the lane-weighted road length within each GOES cell, we derived an index that reflects both total roadway extent and lane capacity.

3. Methods

3.1. Surface Urban Heat Island Intensity (SUHII)

We calculate the Surface Urban Heat Island Intensity (SUHII) for each urban GOES grid cell (Figure 1b) on an hourly basis, focusing on the warm season from 2018 to 2024. First, we compute the average rural LST for each hour by aggregating all rural GOES grid cells identified in previous section. This rural baseline captures the reference temperature outside the urban region. We then subtract this hourly rural average from the corresponding hourly LST in each urban grid cell to obtain SUHII (Bechtel et al., 2019; Lee, 2024; Z. Liu et al., 2022; Voogt & Oke, 2003). Mathematically, this is represented as Equation 1.

$$\mathrm{SUHII}(i,t) = \mathrm{LST}_{\mathrm{urban}}(i,t) - \mathrm{LST}_{\mathrm{rural}}(t) \quad (1)$$

In Equation 1, i denote the index of an urban GOES grid cell, and t representing the hourly time step. By quantifying the temperature difference between urban and rural areas, SUHII provides a clear measure of the urban heat island's magnitude and variability over time.

3.2. Generalized Additive Models (GAM)

We employ Generalized Additive Models (GAMs) to examine how traffic speed influences SUHII (Hastie, 2017; Wood, 2017). GAMs are particularly suited for this analysis because they can flexibly capture nonlinear relationships without imposing a strict parametric form. In our setup, we treat SUHII as the response variable and traffic speed as the primary predictor. Given SUHII's pronounced diurnal cycle (Lai et al., 2018; Lee, 2024; Z. Liu et al., 2022), we also include hour of day as a predictor to ensure that any estimated effect of traffic speed is evaluated at comparable times of day. Mathematically, for each grid cell i and time t, we fit the model as in Equation 2.

$$\mathrm{SUHII}_i(t) = \beta_i + s_1(\mathrm{SPEED}_i(t)) + s_2(\mathrm{HOD}(t)) + \varepsilon_i(t) \quad (2)$$

The terms s_1 and s_2 represent smooth functions, specifically implemented as thin-plate regression splines using the mgcv package in R (Wood, 2001). $\mathrm{SPEED}_i(t)$ represent the average CTA bus speed within the grid cell and $\mathrm{HOD}(t)$ represent the local hour of the day. β_i is the intercept and $\varepsilon_i(t)$ is the error term. We set the basis dimension of $k = 8$ for each smoother $s(\cdot)$, which constrains the maximum possible flexibility of the spline fit. The smoothness penalties, which prevent excessive spline complexity, were automatically estimated by the GAM fitting process via Restricted Maximum Likelihood (REML), also implemented directly within the mgcv package. This procedure ensures an optimal balance between model complexity and generalization. By including hour of day as a separate smooth term, the partial dependence of traffic speed on SUHII can be interpreted as its effect independent from the time of day, thereby providing a more accurate assessment of how congestion contributes to urban heat.

We emphasize that GAM analysis is inherently correlational. While GAMs effectively isolate individual predictor effects after controlling for other variables, they do not directly imply causation due to their observational nature. Additional physical or mechanistic modeling would be necessary to confirm direct causal pathways.

3.3. Empirical Orthogonal Functions (EOF)

To address potential collinearity among our five predictors (canopy cover, EVI, building area, road length, population), we employ Empirical Orthogonal Function (EOF) analysis (Hannachi et al., 2007; K.-Y. Kim & North, 1998, 1999; North, 1984). These five factors were chosen based on their established roles in influencing urban heat island dynamics: vegetation (canopy cover, EVI) affects local cooling via shading and evapotranspiration (Melaas et al., 2016; Sekertekin & Zadbagher, 2021), building density and road networks influence heat retention and emission (Patriota et al., 2024; Xu et al., 2024), and population density serves as a proxy for anthropogenic heat (Apriana & Syahrani, 2022; S. Peng et al., 2012). Each predictor is stored as a single vector—one element per grid cell—yielding a data matrix X of size $N \times V$, where N is the number of observation (GOES grid cell) and V is the number of variables. The EOF decomposition then represents X as a sum of orthogonal modes:

$$X = \sum_{k=1}^{K} PC_k \cdot \mathrm{EOF}_k \quad (3)$$

where EOF_k is the kth EOF mode and PC_k is its principal component for each of the N grid cells. By design, these modes are mutually orthogonal, thereby isolating distinct patterns of variability and mitigating the effects of collinearity among the predictors.

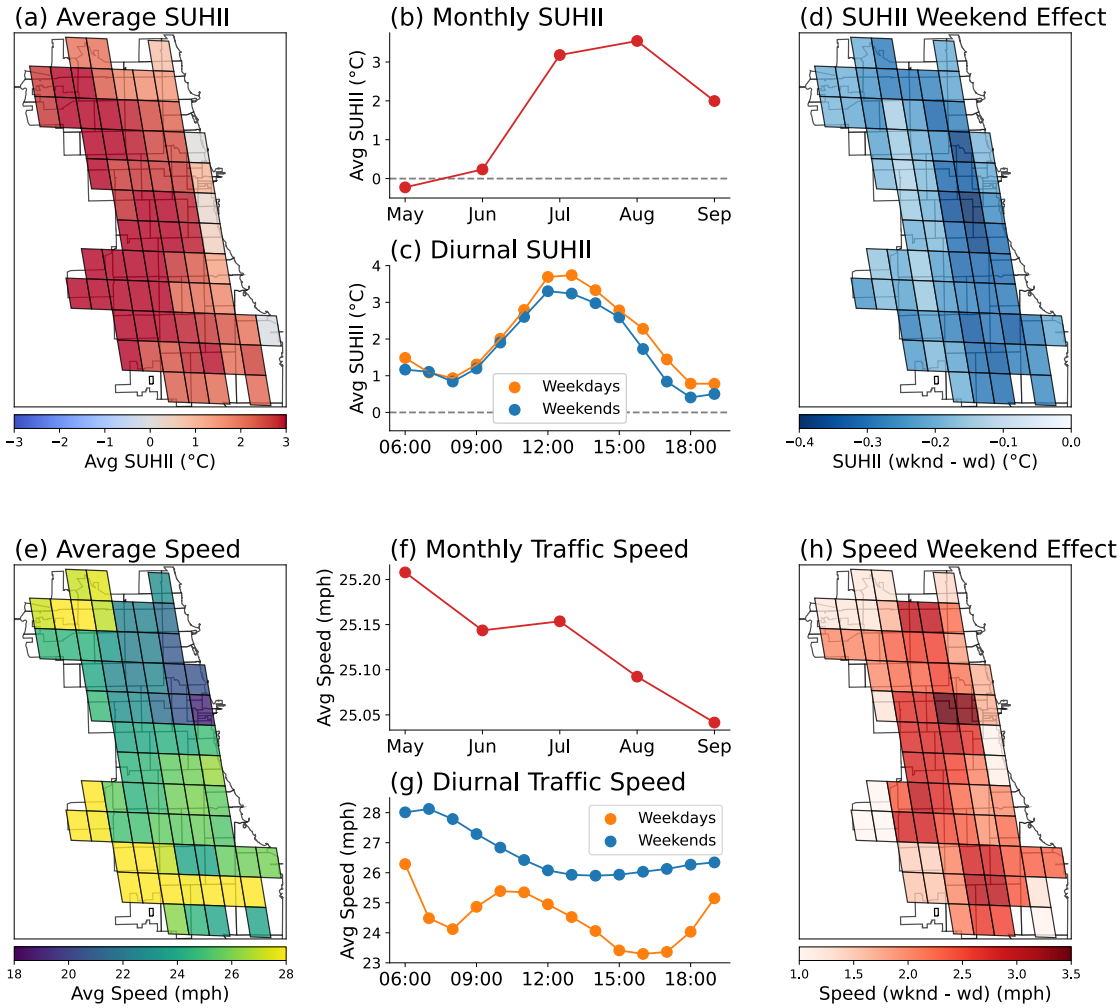

Figure 2. (a) Spatial pattern of average SUHII over Chicago region. (b) Monthly averaged SUHII. (c) Diurnal cycle of SUHII from 6 a.m. to 7 p.m. (d) Spatial distribution of average weekend effect (weekend–weekday) of SUHII over study region. (e–h) Same as (a–d), but for traffic speed, rather than SUHII.

4. Results

4.1. General SUHII and Traffic Speed Patterns

We first examine the spatial distribution of SUHII, as well as its seasonal (monthly) and diurnal cycles (Figures 2a–2c). Geographically, SUHII is lower on the eastern side of Chicago near Lake Michigan, due to cooler lake breezes moderating surface temperatures. Our difference-in-differences analysis quantitatively confirmed this cooling effect, showing that lakeshore areas (within ~4 km of Lake Michigan) are significantly cooler by approximately 0.7°C (p = 0.0005) compared to inland grid cells, consistent with previous studies documenting lake breeze effects on urban heat islands (Lee & Berkelhammer, 2024). Monthly patterns show a lower SUHII in May and a peak in August, which typical for cities surrounded by intensive agricultural. In spring, when croplands lie fallow, rural areas can exhibit higher land surface temperatures, reducing the contrast with urban zones (Lee, 2024; Wang et al., 2018; Wickham et al., 2012).

Diurnally, SUHII peaks at midday under maximum solar radiation and shows a secondary increase before sunrise (around 6 a.m.) due to residual heat released from urban surfaces overnight. Weekdays exhibit a higher afternoon SUHII than weekends, likely reflecting intensified anthropogenic activities such as traffic and building operations throughout the city. This weekend effect is consistent across the entire study region, with all grid cells showing higher SUHII on weekdays. Spatial correlation between the weekend effect (Figure 2d) and the average SUHII (Figure 2a) is weak (R = 0.2), suggesting different underlying mechanisms for these two metrics. Notably,

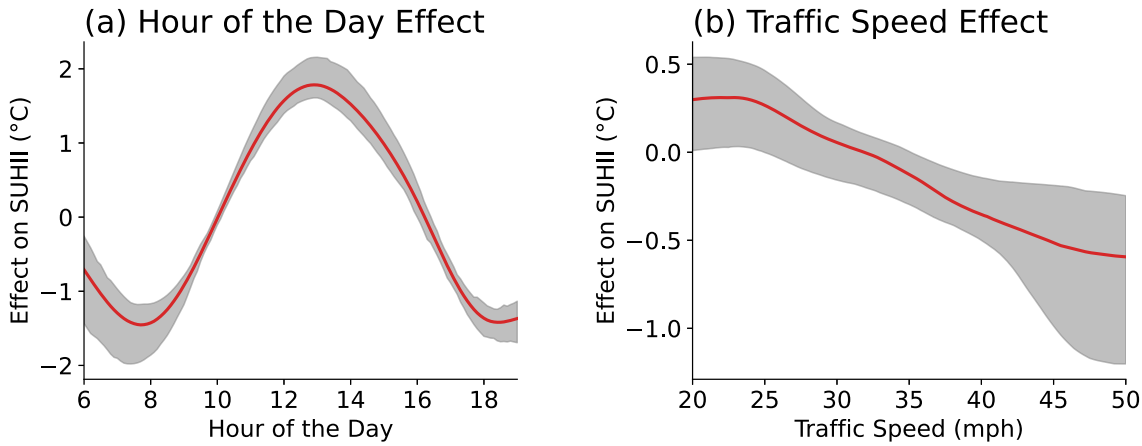

Figure 3. (a) Partial dependence function of hour of the day on SUHII. Red line denotes the effect averaged over all grid points, while the grey area represents the spread between different grid points (Q1–Q3). (b) Same as (a), but for the traffic speed.

weekend SUHII can be lower in certain neighborhoods due to a reduction in both traffic and building operations, and cells adjacent to Lake Michigan consistently remain cooler—presumably due to the onshore breeze—while downtown areas exhibit higher baseline anthropogenic heat.

Examining the traffic speed data (Figures 2e–2h) reveals a consistent pattern of lower speeds in the urban core and higher speeds on the outskirts. Temporally, speeds remain relatively stable from month to month but show a pronounced diurnal cycle, dropping sharply around 8 a.m. and 4 p.m. on weekdays due to commuter rush hours. This pattern is largely absent on weekends, when typical commuting routines do not apply. The presence of these varying traffic cycles is beneficial for our regression model, as it provides the temporal diversity needed to isolate and quantify the effect of traffic speed on SUHII.

The spatial weekend effect of traffic speed (Figure 2h) is most prevalent near downtown Chicago and is correlated with average speed ($R = -0.47$, $p = 1 \times 10^{-5}$), total road length ($R = 0.49$, $p = 9 \times 10^{-6}$), and building area fraction ($R = 0.48$, $p = 9 \times 10^{-6}$). These findings indicate that weekend traffic speed differences are most pronounced in areas with extensive road infrastructure, dense building coverage, and already slower baseline traffic. Comparing the weekend effect on SUHII and on traffic speed yields no significant statistical relationship, implying that factors beyond traffic dynamics contribute to SUHII's weekend effect.

4.2. Impact of Traffic Speed on SUHII

We apply a GAM regression model to each GOES grid cell within the urban region, using SUHII as the response variable and hour of day plus traffic speed as predictors. For each pixel, we derive partial dependence functions from the fitted models, then average them across all pixels to illustrate the effects of hour of day and traffic speed (Figure 3). The hour-of-day effect shown in Figure 3a represents the isolated contribution of diurnal timing after statistically controlling for traffic speed within the GAM. Thus, Figure 3a specifically illustrates the GAM-derived isolated diurnal signal, rather than the raw observed diurnal variation itself, reflecting the effectiveness of the GAM approach in separating temporal effects from other influences. Examining traffic speed, we observe a statistically significant negative correlation with SUHII (urban-rural temperature difference), meaning higher speeds are associated with smaller differences between urban and rural temperatures, whereas lower speeds (congestion) correlate with larger temperature differences. Specifically, a 10 mph decrease in traffic speed is associated with a 0.36°C increase in SUHII.

Importantly, this relationship is observational and associative rather than causal, as other urban characteristics, such as construction or waste heat, are not included in the model which might also influence this correlation. The relatively narrow range of the traffic-speed partial dependence plot (Figure 3b) compared to dependence of diurnal cycle (Figure 3a) arises precisely because our GAM explicitly isolates the traffic effect from the dominant diurnal variation. Thus, the magnitude shown represents the specific incremental association of traffic speed with SUHII, independent of the much larger diurnal variability captured separately by the hour-of-day term. Within the typical speed range of 20–50 mph in Chicago, this can amount to a 1.1°C difference. Given that the average

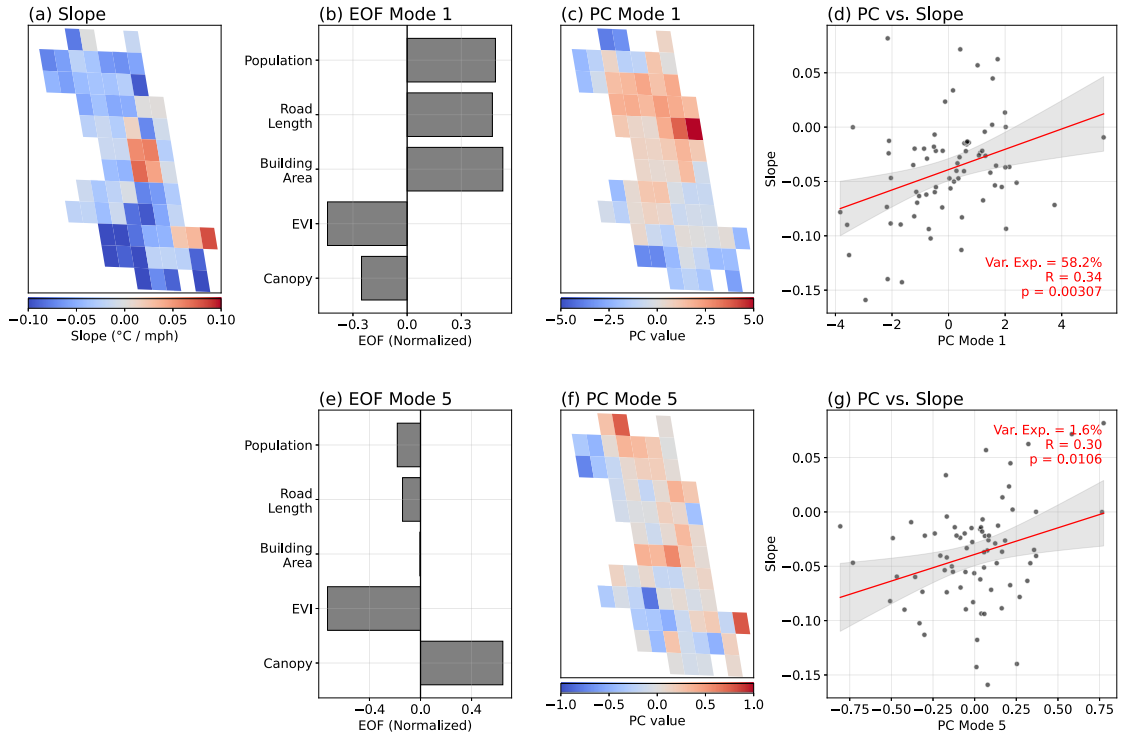

Figure 4. (a) Spatial distribution of the slope (°C per mph) describing how traffic speed affects SUHII; negative values indicate increased SUHII when traffic slows. (b) Loadings of EOF Mode 1 (58.2% of variance). (c) Principal component (PC) values for Mode 1, and (d) correlation of PC Mode 1 versus slope (red line shows linear fit and ±1 std). (e) Loadings of EOF Mode 5 (1.6% of variance), (f) corresponding PC Mode 5 map, and (g) PC versus slope correlation plot.

SUHII is around 1.8°C, this suggests that variations in traffic speed can significantly influence Chicago's overall urban heat island intensity.

4.3. Factors Influencing Traffic's Effect on SUHII

Although the citywide average suggests a 0.36°C rise of SUHII is associated with 10 mph reduction in traffic speed, the actual effect varies notably across Chicago. Figure 4a maps the local slope of this relationship for each 2 km grid cell, revealing that while most cells have a negative slope (indicating SUHII increases when traffic slows), roughly 14% show weaker or even positive slopes—evidence that the congestion-driven heat signal is far from uniform. These spatial discrepancies likely reflect variations in land-surface characteristics and other anthropogenic heat sources that can either amplify or suppress traffic-induced warming.

To understand these differences, we examined five potential explanatory factors: canopy cover, EVI, building area, road length, and population. Because these variables can be strongly interrelated (e.g., dense building footprints often coincide with fewer trees), we used Empirical Orthogonal Function (EOF) analysis. Of the five EOF modes produced, EOF Mode 1 and EOF Mode 5 correlate strongly with the slope shown in Figure 4a, whereas Modes 2–4 do not and are therefore excluded from further discussion.

EOF Mode 1 (Figure 4b) accounts for 58.2% of the total variance in canopy cover, EVI, building area, road length, and population. Here, canopy cover and EVI both loads negatively, meaning that areas with limited vegetation load positively on the corresponding principal component (PC Mode 1, Figure 4c). A positive correlation between PC Mode 1 and the slope (Figure 4d) indicates that neighborhoods with higher vegetation see a stronger SUHII response when traffic slows, due to lower baseline anthropogenic heat emissions making traffic-related heat more distinguishable. Conversely, areas with lower canopy and EVI (more built areas) exhibit more moderate slopes. This is because in denser built-up areas, the presence of additional heat sources (e.g., waste heat from air-conditioning) may overshadow traffic's influence, reducing the observed coupling between congestion and SUHII.

EOF Mode 5 (Figure 4e), which explains 1.6% of the variance, captures a less common pattern featuring relatively high canopy cover but low EVI. Although canopy cover and EVI are strongly correlated overall ($R = 0.85$), this

small fraction of variance highlights places where the two metrics diverge. The corresponding principal component map (Figure 4f) again correlates positively with the slope (Figure 4g), suggesting that tree cover (as opposed to overall EVI or "greenness") can mitigate the localized impact of congestion-related heat. Because Mode 5 describes under 2% of total variance, it applies to only a small subset of urban conditions—but still underscores how different vegetation types can confer resilience.

Our additional spatial difference analysis, which compared grid cells categorized based on the 25th and 75th percentiles of urban characteristics, provides further quantitative support for the EOF-based results. Specifically, grid cells with high canopy cover were significantly cooler (0.65°C; $p = 0.0004$). Conversely, grid cells with high population density were significantly warmer (0.5°C; $p = 0.009$), while high building-density areas showed marginally higher temperatures (0.34°C; $p = 0.08$). These results numerically reinforce the importance of vegetation cover, high population and building densities in modeling urban heat. Nevertheless, there are limitations due to collinearity among these urban characteristics, complicating the precise attribution of temperature differences. In this context, the EOF analysis remains especially valuable, as it explicitly addresses collinearity by identifying distinct modes of variability across multiple correlated urban factors.

5. Summary and Discussion

This study analyzed land surface temperature (LST) data from GOES satellites to calculate the surface urban heat island intensity (SUHII) over urban areas of Chicago. By integrating traffic speed information derived from CTA buses, we explored how changes in traffic speed (or congestion) affect local SUHII. There are three main findings from this work:

- SUHII and traffic speed have distinct diurnal cycles and weekday/weekend patterns. SUHII peaks around noon, while congestion peaks during rush hours. These differences establish the statistical framework to isolate the congestion influence on SUHI.
- Using GAM analysis, we found that slower traffic speeds (indicative of congestion) are statistically associated with increased local SUHII. This result underscores an observational correlation rather than direct causation.
- Looking at local characteristics of the impact of traffic in local SUHII, we found that this link is more pronounced in high-vegetation (both canopy cover and EVI) and low-built up areas (including buildings, roads, and population). This is because in these regions, traffic is the dominant waste heat source that can impact SUHII, whereas other sources heat (e.g., waste heat from A/C) are more pronounced in densely built areas.

These findings highlight the connections among urban design, vegetation, human activity, and localized heat patterns, demonstrating that traffic congestion can significantly influence the microclimate in addition to well-studied factors like impervious surfaces and building density.

From a mechanistic perspective, the observed association between traffic congestion and increased SUHII can be explained by the direct emission of anthropogenic heat from vehicles. Traffic-related heat emissions, generated by engine combustion, exhaust, and frictional heating, directly warm the near-surface air and subsequently influence surface temperatures through air-surface heat exchange processes (Fujimoto et al., 2012; Zhu et al., 2017). Under the constraint of surface energy balance, these emissions manifest as measurable increases in surface temperatures, detectable via satellite remote sensing (Sailor, 2011; Z. Yu et al., 2021). Congested conditions amplify these emissions by increasing vehicle density and altering driving behaviors such as frequent acceleration and braking, which produce additional heat per unit road length. Consequently, traffic-induced heat represents a significant and distinct component of urban anthropogenic heating, warranting targeted attention in urban heat mitigation strategies (Husni et al., 2022; Shahmohamadi et al., 2011).

From an environmental science standpoint, recognizing traffic as a distinct heat source adds novelty to traditional SUHI analyses, which often focus on broad land-use characteristics or the role of evapotranspiration. The capacity of traffic to create localized "hot spots" underscores the need for high-resolution data such that citywide averages may overlook areas where congestion consistently elevates temperatures beyond typical urban levels. Such granular insights can inform innovative mitigation measures, such as establishing green corridors along busy routes or fine-tuning transit operations in especially vulnerable neighborhoods.

Beyond purely environmental implications, this work also suggests valuable opportunities for data-driven urban planning. In cities like Chicago, urban planners and other decisionmakers can use traffic-speed data to map communities at higher risk of both thermal stress and air pollution. Implementing strategies to reduce traffic,

adding shade trees or vegetated buffers, and promoting alternative transportation options could alleviate multiple stressors simultaneously. An illustrative example includes shipping and distribution hubs with high truck traffic, where congestion-related emissions can compound local heat and air-quality issues. Moreover, pinpointing where heavy traffic aligns with inadequate green cover allows decisionmakers to target interventions for populations that stand to benefit most.

In conclusion, this work demonstrates that traffic congestion can be a significant, albeit context-dependent, contributor to the urban heat island effect. While it does not diminish the importance of broader land-use patterns or building design, it highlights the need to factor traffic conditions into local climate strategies. By integrating high-resolution traffic data with satellite-derived LST measurements, researchers and policymakers can gain a more detailed understanding of how transportation systems interact with the built environment—and more importantly, use this knowledge to guide interventions that balance both mobility and climate resilience goals. Ultimately, integrating traffic data into urban heat research offers a promising pathway toward more adaptive and cooler city planning. While our focus is on Chicago, the methods presented here can be applied to other metropolitan areas with publicly available traffic data and frequent satellite coverage. The magnitude of congestion-related warming may vary by local climate, building density, and land-use practices.

This study is not without limitations. The analysis relies on CTA bus speeds as a proxy for traffic congestion, which, while useful, may not fully capture traffic dynamics on highways, suburban arterials, or roads without bus routes. Future work could incorporate more comprehensive congestion datasets—potentially from GPS-equipped vehicles or mobile navigation apps—to provide broader spatial coverage and finer granularity. Another limitation lies in the identification of factors influencing the coupling between traffic speed and SUHII. While vegetation and built area emerged as significant predictors, other variables (e.g., detailed waste-heat emissions, industrial activities, or localized socioeconomic indicators) may also play important roles but remain challenging to quantify. Further research employing direct physical measurements or causal inference modeling would be necessary to establish whether direct causal pathways exist between traffic congestion (or other factors) and increases in urban heat island intensity. Furthermore, this study used land surface temperatures (LST) rather than near-surface air temperatures to illustrate the effects of congestion. Although LST offers valuable high-resolution insights, vehicle-related heat emissions can have a more direct influence on air temperature at pedestrian level. Acquiring high-resolution air temperature measurements—or effectively modeling them—would likely refine our understanding of traffic's effect on local heat conditions. Lastly, this analysis focuses exclusively on Chicago, a major metropolitan area located in the Midwestern United States. Although we have examined the relationship between SUHI and traffic congestion using bus speed as a proxy, this approach may not directly translate to other cities due to variations in road networks, infrastructure, or urban form. Additionally, the impact of traffic speed on SUHI may differ significantly across other cities in the U.S. or globally. Therefore, expanding this analysis to include additional cities would provide valuable insights and improve the generalizability of our findings.

Conflict of Interest

The authors declare no conflicts of interest relevant to this study.

Data Availability Statement

GOES-16, 17 and 18 data can be found in Amazon Web Service (AWS) repository: https://noaa-goes16.s3.amazonaws.com/index.html, https://noaa-goes17.s3.amazonaws.com/index.html, https://noaa-goes18.s3.amazonaws.com/index.html. Chicago traffic speed data can be downloaded at Chicago Data Portal: https://data.cityofchicago.org/Transportation/Chicago-Traffic-Tracker-Congestion-Estimates-by-Re/t2qc-9pjd/about_data. Chicago building footprint data can also be downloaded at Chicago Data Portal: https://data.cityofchicago.org/Buildings/Building-Footprints-current-/hz9b-7nh8. The road network of Chicago can be downloaded from Chicago Data Portal: https://data.cityofchicago.org/Transportation/Street-Center-Lines/6imu-meau. NOAA C-CAP data for canopy, impervious, and water land cover can be downloaded from C-CAP website (www.coast.noaa.gov/htdata/raster1/landcover/bulkdownload/hires/) (NOAA, 2023). MODIS EVI data can be download from Google Earth Engine (https://developers.google.com/earth-engine/datasets/catalog/MODIS_MOD09GA_006_EVI).

Acknowledgments
This material is based upon work supported by the U.S. Department of Energy, Office of Science, Office of Biological and Environmental Research's Urban Integrated Field Laboratories CROCUS project research activity, under Award Number DE-SC0023226.

References

Apriana, M., & Syahrani, E. (2022). Land surface temperature and its relationship to population density. *Journal of Applied Geospatial Information*, *6*(1), 569–575. https://doi.org/10.30871/jagi.v6i1.1936

Baniassadi, A., Heusinger, J., & Sailor, D. J. (2018). Energy efficiency vs resiliency to extreme heat and power outages: The role of evolving building energy codes. *Building and Environment*, *139*, 86–94. https://doi.org/10.1016/j.buildenv.2018.05.024

Baniassadi, A., & Sailor, D. J. (2018). Synergies and trade-offs between energy efficiency and resiliency to extreme heat–A case study. *Building and Environment*, *132*, 263–272. https://doi.org/10.1016/j.buildenv.2018.01.037

Beale, C., Norouzi, H., Sharifnezhadazizi, Z., Bah, A. R., Yu, P., Yu, Y., et al. (2019). Comparison of diurnal variation of land surface temperature from GOES-16 ABI and MODIS instruments. *IEEE Geoscience and Remote Sensing Letters*, *17*(4), 572–576. https://doi.org/10.1109/lgrs.2019.2930174

Bechtel, B., Demuzere, M., Mills, G., Zhan, W., Sismanidis, P., Small, C., & Voogt, J. (2019). SUHI analysis using local climate zones—A comparison of 50 cities. *Urban Climate*, *28*, 100451. https://doi.org/10.1016/j.uclim.2019.01.005

Chen, F., Zhang, X., & Chen, Z. (2023). Behind climate change: Extreme heat and health cost. *Structural Change and Economic Dynamics*, *64*, 101–110. https://doi.org/10.1016/j.strueco.2022.12.007

Chen, P.-Y., Fedosejevs, G., Tiscareño-LóPez, M., & Arnold, J. G. (2006). Assessment of MODIS-EVI, MODIS-NDVI and VEGETATION-NDVI composite data using agricultural measurements: An example at corn fields in western Mexico. *Environmental Monitoring and Assessment*, *119*(1–3), 69–82. https://doi.org/10.1007/s10661-005-9006-7

Cui, F., Hamdi, R., Yuan, X., He, H., Yang, T., Kuang, W., et al. (2021). Quantifying the response of surface urban heat island to urban greening in global north megacities. *Science of the Total Environment*, *801*, 149553. https://doi.org/10.1016/j.scitotenv.2021.149553

Deilami, K., Kamruzzaman, M., & Liu, Y. (2018). Urban heat island effect: A systematic review of spatio-temporal factors, data, methods, and mitigation measures. *International Journal of Applied Earth Observation and Geoinformation*, *67*, 30–42. https://doi.org/10.1016/j.jag.2017.12.009

Ebi, K. L., Capon, A., Berry, P., Broderick, C., de Dear, R., Havenith, G., et al. (2021). Hot weather and heat extremes: Health risks. *The Lancet*, *398*(10301), 698–708. https://doi.org/10.1016/s0140-6736(21)01208-3

Fujimoto, A., Saida, A., & Fukuhara, T. (2012). A new approach to modeling vehicle-induced heat and its thermal effects on road surface temperature. *Journal of Applied Meteorology and Climatology*, *51*(11), 1980–1993. https://doi.org/10.1175/jamc-d-11-0156.1

Hannachi, A., Jolliffe, I. T., & Stephenson, D. B. (2007). Empirical orthogonal functions and related techniques in atmospheric science: A review. *International Journal of Climatology*, *27*(9), 1119–1152. https://doi.org/10.1002/joc.1499

Hastie, T. J. (2017). Generalized additive models. In *Statistical models in S* (pp. 249–307). Routledge.

Hayhoe, K., Sheridan, S., Kalkstein, L., & Greene, S. (2010). Climate change, heat waves, and mortality projections for Chicago. *Journal of Great Lakes Research*, *36*, 65–73. https://doi.org/10.1016/j.jglr.2009.12.009

Hou, H., Su, H., Yao, C., & Wang, Z.-H. (2023). Spatiotemporal patterns of the impact of surface roughness and morphology on urban heat island. *Sustainable Cities and Society*, *92*, 104513. https://doi.org/10.1016/j.scs.2023.104513

Husni, E., Prayoga, G. A., Tamba, J. D., Retnowati, Y., Fauzandi, F. I., Yusuf, R., & Yahya, B. N. (2022). Microclimate investigation of vehicular traffic on the urban heat island through IoT-Based device. *Heliyon*, *8*(11), e11739. https://doi.org/10.1016/j.heliyon.2022.e11739

Justice, C., Townshend, J., Vermote, E., Masuoka, E., Wolfe, R., Saleous, N., et al. (2002). An overview of MODIS Land data processing and product status. *Remote Sensing of Environment*, *83*(1–2), 3–15. https://doi.org/10.1016/s0034-4257(02)00084-6

Kaiser, R., Le Tertre, A., Schwartz, J., Gotway, C. A., Daley, W. R., & Rubin, C. H. (2007). The effect of the 1995 heat wave in Chicago on all-cause and cause-specific mortality. *American Journal of Public Health*, *97*, S158–S162. https://doi.org/10.2105/ajph.2006.100081

Khosla, R., Jani, A., & Perera, R. (2021). *Health risks of extreme heat* (Vol. 375). British Medical Journal Publishing Group. https://doi.org/10.1136/bmj.n2438

Kim, K.-Y., & North, G. R. (1998). EOF-based linear prediction algorithm: Theory. *Journal of Climate*, *11*(11), 3046–3056. https://doi.org/10.1175/1520-0442(1998)011<3046:eblpat>2.0.co;2

Kim, K.-Y., & North, G. R. (1999). EOF-based linear prediction algorithm: Examples. *Journal of Climate*, *12*(7), 2076–2092. https://doi.org/10.1175/1520-0442(1999)012<2076:eblpae>2.0.co;2

Kim, S. W., & Brown, R. D. (2021). Urban heat island (UHI) intensity and magnitude estimations: A systematic literature review. *Science of the Total Environment*, *779*, 146389. https://doi.org/10.1016/j.scitotenv.2021.146389

Klinenberg, E. (2015). *Heat wave: A social autopsy of disaster in Chicago*. University of Chicago Press.

Kong, G., Peng, J., & Corcoran, J. (2025). Modelling urban heat island effects: A global analysis of 216 cities using machine learning techniques. *Computational Urban Science*, *5*(1), 1–12. https://doi.org/10.1007/s43762-025-00178-w

Lai, J., Zhan, W., Huang, F., Voogt, J., Bechtel, B., Allen, M., et al. (2018). Identification of typical diurnal patterns for clear-sky climatology of surface urban heat islands. *Remote Sensing of Environment*, *217*, 203–220. https://doi.org/10.1016/j.rse.2018.08.021

Lee, J. (2024). Assessment of US urban surface temperature using GOES-16 and GOES-17 data: Urban heat island and temperature inequality. *Weather, Climate, and Society*, *16*(2), 315–329. https://doi.org/10.1175/wcas-d-23-0129.1

Lee, J., & Berkelhammer, M. (2024). Observational constraints on the spatial effect of greenness and Canopy Cover on Urban Heat in a major midlatitude city. *Geophysical Research Letters*, *51*(21), e2024GL110847. https://doi.org/10.1029/2024gl110847

Lee, J., & Dessler, A. E. (2022). The impact of neglecting climate change and variability on ERCOT's forecasts of electricity demand in Texas. *Weather, Climate, and Society*, *14*(2), 499–505. https://doi.org/10.1175/wcas-d-21-0140.1

Lee, J., & Dessler, A. E. (2023). Future temperature-related deaths in the US: The impact of climate change, demographics, and adaptation. *GeoHealth*, *7*(8), e2023GH000799. https://doi.org/10.1029/2023gh000799

Li, X., Zhou, Y., Yu, S., Jia, G., Li, H., & Li, W. (2019). Urban heat island impacts on building energy consumption: A review of approaches and findings. *Energy*, *174*, 407–419. https://doi.org/10.1016/j.energy.2019.02.183

Liu, W., You, H., & Dou, J. (2009). Urban-rural humidity and temperature differences in the Beijing area. *Theoretical and Applied Climatology*, *96*(3–4), 201–207. https://doi.org/10.1007/s00704-008-0024-6

Liu, Z., Zhan, W., Lai, J., Bechtel, B., Lee, X., Hong, F., et al. (2022). Taxonomy of seasonal and diurnal clear-sky climatology of surface urban heat island dynamics across global cities. *ISPRS Journal of Photogrammetry and Remote Sensing*, *187*, 14–33. https://doi.org/10.1016/j.isprsjprs.2022.02.019

Louiza, H., Zéroual, A., & Djamel, H. (2015). Impact of the transport on the urban heat island. *International Journal of Traffic and Transportation Engineering*, *5*(3), 252–263. https://doi.org/10.7708/ijtte.2015.5(3).03

Luo, S., Gu, X., Guan, Y., Wang, L., Slater, L. J., Kong, D., et al. (2025). Hot weather amplifies the urban dry island effect, especially in wetter climates. *Journal of Geophysical Research: Atmospheres*, *130*(6), e2024JD043224. https://doi.org/10.1029/2024jd043224

Melaas, E. K., Wang, J. A., Miller, D. L., & Friedl, M. A. (2016). Interactions between urban vegetation and surface urban heat islands: A case study in the Boston metropolitan region. *Environmental Research Letters*, *11*(5), 054020. https://doi.org/10.1088/1748-9326/11/5/054020

Morakinyo, T. E., Ren, C., Shi, Y., Lau, K. K.-L., Tong, H.-W., Choy, C.-W., & Ng, E. (2019). Estimates of the impact of extreme heat events on cooling energy demand in Hong Kong. *Renewable Energy*, *142*, 73–84. https://doi.org/10.1016/j.renene.2019.04.077

NOAA. (2023). Coastal change analysis program (C-CAP) high-resolution land cover. Retrieved from www.coast.noaa.gov/htdata/raster1/landcover/bulkdownload/hires/

North, G. R. (1984). Empirical orthogonal functions and normal modes. *Journal of the Atmospheric Sciences*, *41*(5), 879–887. https://doi.org/10.1175/1520-0469(1984)041<0879:eofanm>2.0.co;2

Paschalis, A., Chakraborty, T., Fatichi, S., Meili, N., & Manoli, G. (2021). Urban forests as main regulator of the evaporative cooling effect in cities. *AGU Advances*, *2*(2), e2020AV000303. https://doi.org/10.1029/2020av000303

Patriota, E. G., Bertrand, G. F., Almeida, C. D. N., Claudino, C. M. D. A., & Coelho, V. H. R. (2024). Heat the road again! Twenty years of surface urban heat island intensity (SUHII) evolution and forcings in 21 tropical metropolitan regions in Brazil from remote sensing analyses. *Sustainable Cities and Society*, *113*, 105629. https://doi.org/10.1016/j.scs.2024.105629

Peng, S., Piao, S., Ciais, P., Friedlingstein, P., Ottle, C., Bréon, F.-M., et al. (2012). Surface urban heat island across 419 global big cities. *Environmental Science & Technology*, *46*(2), 696–703. https://doi.org/10.1021/es2030438

Peng, W., Wang, R., Duan, J., Gao, W., & Fan, Z. (2022). Surface and canopy urban heat islands: Does urban morphology result in the spatiotemporal differences? *Urban Climate*, *42*, 101136. https://doi.org/10.1016/j.uclim.2022.101136

Phiri, D., Simwanda, M., Salekin, S., Nyirenda, V. R., Murayama, Y., & Ranagalage, M. (2020). Sentinel-2 data for land cover/use mapping: A review. *Remote Sensing*, *12*(14), 2291. https://doi.org/10.3390/rs12142291

Rizwan, A. M., Dennis, L. Y., & Chunho, L. (2008). A review on the generation, determination and mitigation of Urban Heat Island. *Journal of Environmental Sciences*, *20*(1), 120–128. https://doi.org/10.1016/s1001-0742(08)60019-4

Rumora, L., Miler, M., & Medak, D. (2020). Impact of various atmospheric corrections on Sentinel-2 land cover classification accuracy using machine learning classifiers. *ISPRS International Journal of Geo-Information*, *9*(4), 277. https://doi.org/10.3390/ijgi9040277

Sailor, D. J. (2011). A review of methods for estimating anthropogenic heat and moisture emissions in the urban environment. *International Journal of Climatology*, *31*(2), 189–199. https://doi.org/10.1002/joc.2106

Sekertekin, A., & Zadbagher, E. (2021). Simulation of future land surface temperature distribution and evaluating surface urban heat island based on impervious surface area. *Ecological Indicators*, *122*, 107230. https://doi.org/10.1016/j.ecolind.2020.107230

Sen, S. (2025). Geoengineering cities with reflective and pervious surfaces. In *Geoengineering and climate change: Methods, risks, and governance* (pp. 231–245). https://doi.org/10.1002/9781394204847.ch14

Shahmohamadi, P., Che-Ani, A., Maulud, K., Tawil, N. M., & Abdullah, N. (2011). The impact of anthropogenic heat on formation of urban heat island and energy consumption balance. *Urban Studies Research*, *2011*(1), 497524. https://doi.org/10.1155/2011/497524

Shao, L., Liao, W., Li, P., Luo, M., Xiong, X., & Liu, X. (2023). Drivers of global surface urban heat islands: Surface property, climate background, and 2D/3D urban morphologies. *Building and Environment*, *242*, 110581. https://doi.org/10.1016/j.buildenv.2023.110581

Singh, C., Jain, G., Sukhwani, V., & Shaw, R. (2021). Losses and damages associated with slow-onset events: Urban drought and water insecurity in Asia. *Current Opinion in Environmental Sustainability*, *50*, 72–86. https://doi.org/10.1016/j.cosust.2021.02.006

Son, N., Chen, C., Chen, C., Minh, V., & Trung, N. (2014). A comparative analysis of multitemporal MODIS EVI and NDVI data for large-scale rice yield estimation. *Agricultural and Forest Meteorology*, *197*, 52–64. https://doi.org/10.1016/j.agrformet.2014.06.007

Teufel, B., Sushama, L., Poitras, V., Dukhan, T., Bélair, S., Miranda-Moreno, L., et al. (2021). Impact of COVID-19-related traffic slowdown on urban heat characteristics. *Atmosphere*, *12*(2), 243. https://doi.org/10.3390/atmos12020243

Topaloğlu, R. H., Sertel, E., & Musaoğlu, N. (2016). Assessment of classification accuracies of Sentinel-2 and Landsat-8 data for land cover/use mapping. *The International Archives of the Photogrammetry, Remote Sensing and Spatial Information Sciences*, *41*, 1055–1059. https://doi.org/10.5194/isprs-archives-xli-b8-1055-2016

Voogt, J. A., & Oke, T. R. (2003). Thermal remote sensing of urban climates. *Remote Sensing of Environment*, *86*(3), 370–384. https://doi.org/10.1016/s0034-4257(03)00079-8

Wang, Y.-C., Hu, B. K., Myint, S. W., Feng, C.-C., Chow, W. T., & Passy, P. F. (2018). Patterns of land change and their potential impacts on land surface temperature change in Yangon, Myanmar. *Science of the Total Environment*, *643*, 738–750. https://doi.org/10.1016/j.scitotenv.2018.06.209

Wickham, J. D., Wade, T. G., & Riitters, K. H. (2012). Comparison of cropland and forest surface temperatures across the conterminous United States. *Agricultural and Forest Meteorology*, *166*, 137–143. https://doi.org/10.1016/j.agrformet.2012.07.002

Wilson, B., & Chakraborty, A. (2019). Mapping vulnerability to extreme heat events: Lessons from metropolitan Chicago. *Journal of Environmental Planning and Management*, *62*(6), 1065–1088. https://doi.org/10.1080/09640568.2018.1462475

Wood, S. N. (2001). mgcv: GAMs and generalized ridge regression for R. *R News*, *1*(2), 20–25.

Wood, S. N. (2017). *Generalized additive models: An introduction with R*. Chapman and Hall/CRC.

Xu, D., Wang, Y., Zhou, D., Wang, Y., Zhang, Q., & Yang, Y. (2024). Influences of urban spatial factors on surface urban heat island effect and its spatial heterogeneity: A case study of Xi'an. *Building and Environment*, *248*, 111072. https://doi.org/10.1016/j.buildenv.2023.111072

Yang, B., Liu, H., Kang, E. L., Hawthorne, T. L., Tong, S. T., Shu, S., & Xu, M. (2022). Traffic restrictions during the 2008 Olympic Games reduced urban heat intensity and extent in Beijing. *Communications Earth & Environment*, *3*(1), 105. https://doi.org/10.1038/s43247-022-00427-4

Yu, Y., Tarpley, D., Privette, J. L., Flynn, L. E., Xu, H., Chen, M., et al. (2011). Validation of GOES-R satellite land surface temperature algorithm using SURFRAD ground measurements and statistical estimates of error properties. *IEEE Transactions on Geoscience and Remote Sensing*, *50*(3), 704–713. https://doi.org/10.1109/tgrs.2011.2162338

Yu, Y., Tarpley, D., Privette, J. L., Goldberg, M. D., Raja, M. R. V., Vinnikov, K. Y., & Xu, H. (2008). Developing algorithm for operational GOES-R land surface temperature product. *IEEE Transactions on Geoscience and Remote Sensing*, *47*(3), 936–951.

Yu, Y., & Yu, P. (2020). Land surface temperature product from the GOES-R series. In *The GOES-R Series* (pp. 133–144). Elsevier.

Yu, Z., Hu, L., Sun, T., Albertson, J., & Li, Q. (2021). Impact of heat storage on remote-sensing based quantification of anthropogenic heat in urban environments. *Remote Sensing of Environment*, *262*, 112520. https://doi.org/10.1016/j.rse.2021.112520

Zhang, X., Chen, N., Sheng, H., Ip, C., Yang, L., Chen, Y., et al. (2019). Urban drought challenge to 2030 sustainable development goals. *Science of the Total Environment*, *693*, 133536. https://doi.org/10.1016/j.scitotenv.2019.07.342

Zhu, R., Wong, M. S., Guilbert, É., & Chan, P.-W. (2017). Understanding heat patterns produced by vehicular flows in urban areas. *Scientific Reports*, *7*(1), 16309. https://doi.org/10.1038/s41598-017-15869-6